Comparative Analysis of DDR and DAR IMPATT Diodes for Wide Frequency Band

ALEXANDER ZEMLIAK[1,3], FERNANDO REYES[2], JAIME CID[2], SERGIO VERGARA[2]
EVGENY MACHUSSKIY[3]
[1]Department of Physics and Mathematics
[2]Department of Electronics
Autonomous University of Puebla
Av. San Claudio y Rio Verde, Puebla, 72570
MEXICO
[3]Institute of Technical Physics
National Technical University of Ukraine
UKRAINE
azemliak@fcfm.buap.mx

Abstract: - The analysis of Double Drift Region (DDR) and Double Avalanche Region (DAR) IMPATT diodes has been realized on basis of the precise drift-diffusion nonlinear model and special optimization procedure. DDR IMPATT diode includes one avalanche region and two drift regions and DAR IMPATT diode includes two avalanche regions inside the diode and one drift regions both for electrons and holes. The phase delay which was produced by means of the two avalanche regions and the drift region *v* is sufficient to obtain the negative resistance for the wide frequency band. The admittance and energy characteristics of the DAR diode were analyzed in very wide frequency band from 30 up to 360 GHz. Output power level was optimized for the second and third frequency bands near the 220 and 330 GHz.

Key Words: - Implicit numerical scheme, active layer structure analysis, DDR and DAR IMPATT diodes.

1 Introduction

The power generation in short part of millimeter region is one of the important problems of modern microwave electronics. The IMPATT diodes of different structures are used very frequently in microwave systems. The single drift region (SDR) and the DDR IMPATT diodes are very well known and used successfully for the microwave power generation in millimeter region [1-3]. The typical DDR diode structure is shown on Fig. 1 by curve 1,

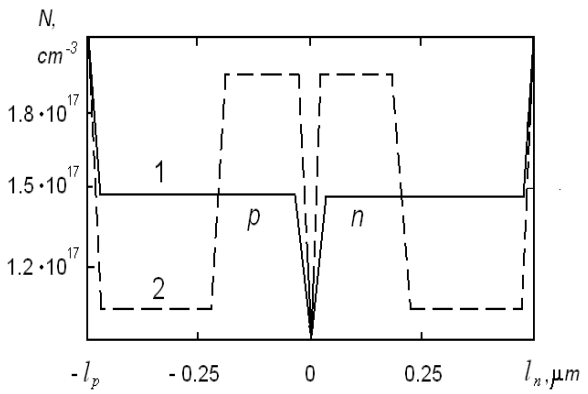

Figure 1. Doping profile for two types of DDR IMPATT diodes: 1- constant doping profile; 2- quasi-Read-type doping profile.

where N is the concentration of donors and acceptors, l is the length of diode active layer. In this type of diodes, the electrical field is strongly distorted when the avalanche current density is sufficiently high. This large space charge density is one of the main reasons for the sharp electrical field gradient along the charge drift path. Because of this field gradient, the space charge avalanche ruins itself and consequently the optimum phase relations degrade between microwave potential and current. This factor is especially important when the IMPATT diode is fed at the maximum current density. The idea to use a complex doping profile semiconductor structure for microwave diode was originally proposed in the first analysis of IMPATT diode by Read [4]. This proposed ideal structure has never been realized till now. However, a modern semiconductor technology provides new possibilities for the fabrication of sub micron semiconductor structures with complex doping profiles. The other proposed DDR type of IMPATT diode doping profile is shown on the Fig. 1 by the curve 2. This type of semiconductor structure can be named as quasi-Read-type structure and this structure provides a concentration of electrical field within the *p-n* junction.

From the famous paper of Read [4] the main idea to obtain the negative resistance was defined on the basis of the phase difference being produced between RF voltage and RF current due to delay in the avalanche build-up process and the transit time of charge carriers. However an IMPATT diode that has double avalanche regions can produce an avalanche delay, which alone can satisfy conditions necessary to generate microwave power [5-7]. This diode can be defined for instance by means of the structure n+pνnp+ in Fig. 2. The DAR diode has two avalanche regions around n+p and np+ junctions and one common drift region. This type of diode was suggested in [5]. The characteristics of this diode were analyzed in DC and RF modes [6-9]. The authors affirm that the avalanche delay produced by each of the thin avalanche regions becomes nearly $\pi/2$, making the total avalanche delay equal to π that is sufficient to produce negative diode resistance and generates the microwave power in millimetric region.

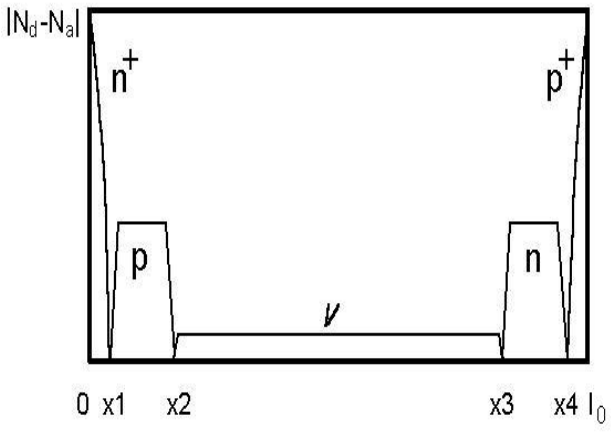

Figure 2. Doping profile of DAR IMPATT diode.

The electric field distribution along the axis *x* for this type of the diode is shown in Fig. 3, curve 2. Curve 1 approximates the electric field distribution for the DDR with constant doping profile diode for comparison.

The characteristics of this diode were analyzed in [9] by means of approximate model. The authors affirm that the diode active properties are produced in many frequency bands for any drift zone width.

Our preliminary analysis that was obtained on basis of the sufficiently precise model [10] contradicts to the results [9]. We need analyze the DAR IMPATT diode for wide frequency band on the basis of this model and optimize the diode structure for the second and third frequency regions.

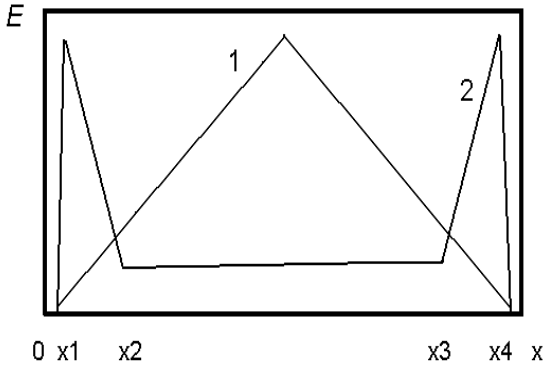

Figure 3. Electric field distribution for DDR IMPATT diode with constant doping profile (1) and DAR IMPATT diode (2).

2 Nonlinear Model

The drift-diffusion model, which is used for the diode analysis, consists of two continuity equations for the electrons and holes, the Poisson equation for the potential distribution in semiconductor structure and necessary boundary conditions as for continuity equations and for the Poisson equation. The principal equations can be presented in next form:

$$\frac{\partial n(x,t)}{\partial t} = \frac{\partial J_n(x,t)}{\partial x} + \alpha_n \left| J_n(x,t) \right| + \alpha_p \left| J_p(x,t) \right|$$
$$\frac{\partial p(x,t)}{\partial t} = -\frac{\partial J_p(x,t)}{\partial x} + \alpha_n \left| J_n(x,t) \right| + \alpha_p \left| J_p(x,t) \right| \quad (1)$$

where

$$J_n(x,t) = n(x,t)\ V_n + D_n \frac{\partial n(x,t)}{\partial x}$$
$$J_p(x,t) = p(x,t)\ V_p - D_p \frac{\partial p(x,t)}{\partial x}$$

n, p are the concentrations of electrons and holes; J_n, J_p are the current densities; α_n, α_p are the ionization coefficients; V_n, V_p are the drift velocities; D_n, D_p are the diffusion coefficients.

The ionization coefficients, drift velocities and diffusion coefficients are the functions of the electric field and temperature in all points of semiconductor structure. The dependence of the ionization coefficients on electric field and temperature can be approximated using the approach described in [11]:

$$\alpha_n(E,T)=\begin{cases}2.6\cdot10^6\, e^{-\left[\left(1.4\cdot10^6+1.3\cdot10^3\cdot T\right)/E\right]} & E<2.4\cdot10^5\\ 6.2\cdot10^5\, e^{-\left[\left(1.05\cdot10^6+1.3\cdot10^3\cdot T\right)/E\right]} & 2.4\cdot10^5<E<5.3\cdot10^5\\ 5.0\cdot10^5\, e^{-\left[\left(0.96\cdot10^6+1.3\cdot10^3\cdot T\right)/E\right]} & E>5.3\cdot10^5\end{cases}$$

$$\alpha_p(E,T)=\begin{cases}2.0\cdot10^6\, e^{-\left[\left(1.95\cdot10^6+1.1\cdot10^3\cdot T\right)/E\right]} & 2.0\cdot10^5<E<5.3\cdot10^5\\ 5.6\cdot10^5\, e^{-\left[\left(1.29\cdot10^6+1.1\cdot10^3\cdot T\right)/E\right]} & E>5.3\cdot10^5\end{cases}$$

The temperature T is expressed in $^\circ C$ and electrical field E is expressed in *V/cm*.

The drift velocities and diffusion coefficients were calculated by means of approximations given in [12-14].

The boundary conditions for this system include concentration and current definition for contact points and can be written as follows:

$$\begin{aligned} &n(0,t)=N_D(0); \qquad p(l_0,t)=N_A(l_0);\\ &J_n(l_0,t)=J_{ns}; \qquad J_p(0,t)=J_{ps}. \end{aligned} \tag{2}$$

where J_{ns}, J_{ps} are the electron current and the hole current for inversely biased *p-n* junction; $N_D(0)$, $N_A(l_0)$ are the concentrations of donors and acceptors at two end space points x = 0 and x = l_0; where l_0 is the length of the active layer of semiconductor structure.

The electrical field distribution in semiconductor structure can be obtained from the Poisson equation. As electron and hole concentrations are functions of the time, therefore, this equation is the time dependent too and time is the equation parameter. The Poisson equation for the above-defined problem has the following normalized form:

$$\frac{\partial E(x,t)}{\partial x}=-\frac{\partial^2 U(x,t)}{\partial x^2}=N_D(x)-N_A(x)+p(x,t)-n(x,t) \tag{3}$$

where $N_D(x)$, $N_A(x)$ are the concentrations of donors and acceptors accordingly, *U(x,t)* is the potential, *E(x,t)* is the electrical field. The boundary conditions for this equation are:

$$U(0,t)=0;\;\; U(l_0,t)=U_0+\sum_{m=1}^{M}U_m\sin\left(\omega mt+\varphi_m\right) \tag{4}$$

where U_0 is the DC voltage on diode contacts; U_m is the amplitude of harmonic number *m* in diode contacts; ω is the fundamental frequency; φ_m is the phase of harmonic number *m*; *M* is the number of harmonics. In this paper we analyze one harmonic regime only (*M=1*) and in this case the phase φ_m can be define as 0. Concrete values of the voltages U_0, U_1 and frequency ω have been defined during the analysis in section 5. Equations (1)-(4) adequately describe processes in the IMPATT diode in a wide frequency band. However, numerical solution of this system of equations is very difficult due to existing of a sharp dependence of equation coefficients on electric field. Explicit numerical schemes have poor stability and require a lot of computing time for good calculation accuracy obtaining [15]. It is more advantageous to use implicit numerical scheme that has a significant property of absolute stability. Computational efficiency and numerical algorithm accuracy are improved by applying the space and the time coordinates symmetric approximation.

After the approximation of the functions and its differentials the system (1) is transformed to the implicit modified Crank-Nicholson numerical scheme. This modification consists of two numerical systems each of them having three-diagonal matrix. These systems are defined by form:

$$\begin{aligned} &-(a_n-b_n)\,n_{i-1}^{k+1}+(1+2a_n)\,n_i^{k+1}-(a_n+b_n)\,n_{i+1}^{k+1}=\\ &\quad a_n\,n_{i-1}^{k}+(1-2a_n)\,n_i^{k}+a_n\,n_{i+1}^{k}+b_n\left(n_{i+1}^{k}-n_{i-1}^{k}\right)\\ &\quad +\alpha_n\left|\tau\cdot V_n\cdot n_i^k+r\cdot D_n\cdot\left(n_{i+1}^k-n_{i-1}^k\right)\right|\\ &\quad +\alpha_p\left|\tau\cdot V_p\cdot p_i^k-r\cdot D_p\cdot\left(p_{i+1}^k-p_{i-1}^k\right)\right| \end{aligned} \tag{5}$$

$$\begin{aligned} &-(a_p+b_p)\,p_{i-1}^{k+1}+(1+2a_p)\,p_i^{k+1}-(a_p-b_p)\,p_{i+1}^{k+1}=\\ &\quad a_p\,p_{i-1}^{k}+(1-2a_p)\,p_i^{k}+a_p\,p_{i+1}^{k}-b_p\left(p_{i+1}^{k}-p_{i-1}^{k}\right)\\ &\quad +\alpha_p\left|\tau\cdot V_p\cdot p_i^k-r\cdot D_p\cdot\left(p_{i+1}^k-p_{i-1}^k\right)\right|\\ &\quad +\alpha_n\left|\tau\cdot V_n\cdot n_i^k+r\cdot D_n\cdot\left(n_{i+1}^k-n_{i-1}^k\right)\right| \end{aligned}$$

i = 1, 2, ... I_1-1; k = 0, 1, 2, ...∞

where $a_{n,p}=\frac{\tau\, D_{n,p}}{2h^2}$; $b_{n,p}=\frac{\tau\, V_{n,p}}{4h}$; $r=\frac{\tau}{2h}$; i is the space coordinate current node number; k is the time coordinate node number; h is the space step; τ is the time step; I_1 is the space node number.

The approximation of the Poisson equation is performed using ordinary finite difference scheme at every time step *k*:

$$U_{i-1}^{k} - 2U_{i}^{k} + U_{i+1}^{k} = h^2\left(N_{Di} - N_{Ai} + p_i^k - n_i^k\right) \quad (6)$$

Numerical algorithm for the calculation of IMPATT diode characteristics consists of the following stages: 1) the voltage is calculated at the diode contacts for every time step by formula (4); 2) the voltage distribution is calculated at every space point from the Poisson equation (6) by factorization method [16], the electrical field distribution along the diode active layer is calculated; 3) the charge carries ionization and drift parameters are calculated in numerical net nodes for the current time step; 4) the system of equations (5) is solved by matrix factorization method taking into account the boundary conditions (2) and electron and hole concentration distributions are calculated for the new time step and then the calculation cycle is repeated for all time steps until the end of the time period; 5) the full current in external circuit is calculated. This process is continued from one period to another until the convergence is achieved by means of the results comparison for the two neighboring periods with the necessary precision. Then all harmonics of external current are calculated by the Fourier transformation $\left(J_0;\ J_m = \left|J_m\right|\exp\left(j\phi_m\right)\right)$; the admittance is calculated for any harmonic number *m* $\left(Y_m = J_m / U_m\right)$ and the power characteristics for all harmonics can be calculated by the following formulas: $\left(P_m = -\frac{1}{2}\ \mathrm{Re}\left(Y_m\right)\ \left|U_m\right|^2;\quad \eta_m = \frac{P_m}{J_0\ U_0}\right)$

3 Optimization Technique

The special optimization algorithm that combines one kind of direct method and a gradient method was used to optimize the output characteristics of DAR diode. To obtain the better solution for the optimum procedure, it is necessary to analyze *N*-dimensional space for *N*=5. The principal vector of optimization parameters consists of five variables $y = \left(y_1, y_2, y_3, y_4, y_5\right)$, where the components will be defined below. The optimization algorithm can be defined by next steps:

1. Given as input two different approximations of two initial points y^0 and y^1.

2. At these points, we start with the gradient method, and have performed some steps. As a result, we have two new points Y^0 and Y^1. This process is reflected by the next equations:

$$\begin{aligned} y^{0,n+1} &= y^{0,n} - \delta_n \cdot \nabla F\left(y^{0,n}\right), \\ y^{1,n+1} &= y^{1,n} - \delta_n \cdot \nabla F\left(y^{1,n}\right), \\ & n=0,1,\text{é},N-1 \\ Y^0 &= y^{0,N},\ \ Y^1 = y^{1,N}, \end{aligned} \quad (7)$$

where *F* is the cost function, and, δ_n is the parameter of the gradient method.

3. We draw a line through two these points, and perform a large step along this line. We have a new point y^{s+1}:

$$y^{s+1} = Y^s + \alpha\left(Y^s - Y^{s-1}\right),\ s = 1, \quad (8)$$

where α is the parameter of the line step.

4. Then we perform some steps from this point by the gradient method, to obtain a new point Y^s:

$$y^{s,n+1} = y^{s,n} - \delta_n \cdot \nabla F\left(y^{s,n}\right), \quad (9)$$

$$s = s + 1,\ Y^s = y^{s,N}.$$

Then step 3 and 4 are repeated with the next values of index *s* (*s* = 2, 3,é).

The optimization process that is presented above cannot find the global minimum of the objective function, but only a local one. To obtain the confidence that we have the better solution of the optimum procedure, it is necessary to investigate N-dimensional space with different initial points. In that case, it is possible to investigate *N*-dimensional volume in more detail. During the optimization process, it is very important to localize the subspace of the *N*-dimension optimization space for more detail analysis. *N*-dimensional space volume of independent parameters is determined approximately on the base of simplified model described in [17] for the first stage of optimization procedure. In that case, a Fourier series approximation of principal functions is used and because of this approximate model, we have a ten times acceleration. After that, on the basis of the precise model described in section 2 we have analyzed the internal structure of the different types of silicon diode.

4 Numerical Scheme Convergence

The numerical scheme for the problem (1) for the DDR IMPATT diode structures was produced some years ago [16]. The scheme analysis showed a very good convergence of the numerical model. The numerical algorithm convergence was obtained during 6ï 8 high frequency periods. On the other hand the careful analysis of numerical model for the DAR diode with the doping profile in Fig.2 shows that the numerical scheme convergence for this type of the doping profile is very slow and the numerical transition process continues many periods to obtain the stationary mode (Fig. 3).

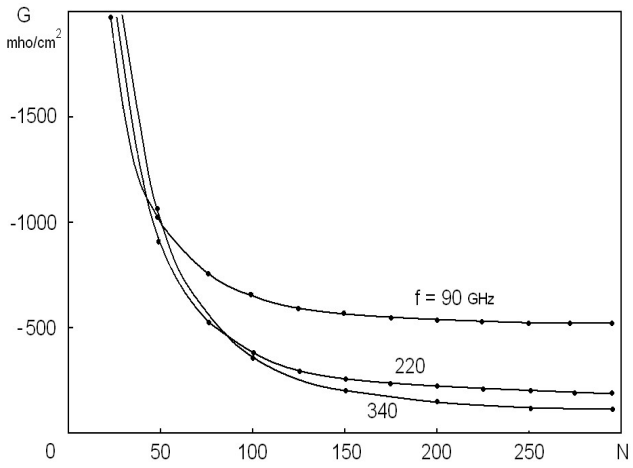

Figure 3. Calculated conductance as function of period number *N*.

The necessary number of the consequent periods depends on the diode width and operating frequency and changes from 30 ï 50 for the frequency band 15 ï 60 GHz up to 150 ï 250 periods for 200 ï 300 GHz. This very slow convergence was stipulated by the asynchronies movement of the electron and hole avalanches along the same drift region *v*. It occurs owing to the different drift velocities of the carriers. This effect provokes a large number of necessary periods and large computer time. This is a specific feature of the analyzed type of diode structure.

5 Results and Discussion

5.1 Admittance characteristics of DDR and DAR diodes

The DDR type of IMPATT diode produces one frequency band only in practice because a very strong losses for high frequency bands. The typical small signal admittance characteristic of DDR diode is shown in Fig. 4.

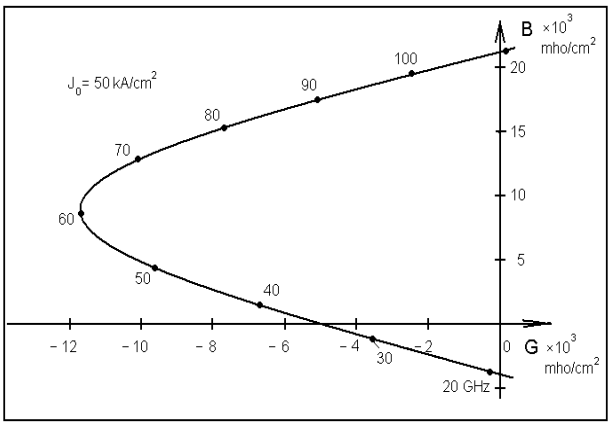

Figure 4. Complex small signal DDR diode admittance (conductance -*G* versus susceptance *B*) for different frequencies.

We can see that DDR IMPATT diode produces microwave power in frequency region between 20 and 110 GHz.

The accurate analysis for DAR IMPATT diode has been made for different values of *p, n* and *v* region width and the different donor and acceptor concentration level. The analysis shows that the active properties of the diode practically are not displayed for more or less significant width of the region *v* [10]. The same doping profile as in [9] gives the negative conductance for very narrow frequency band only as shown in Fig. 5 in conductance versus susceptance plot.

The analysis of DAR IMPATT diode provided some years ago shown interesting and at the same time very surprising results concerning main

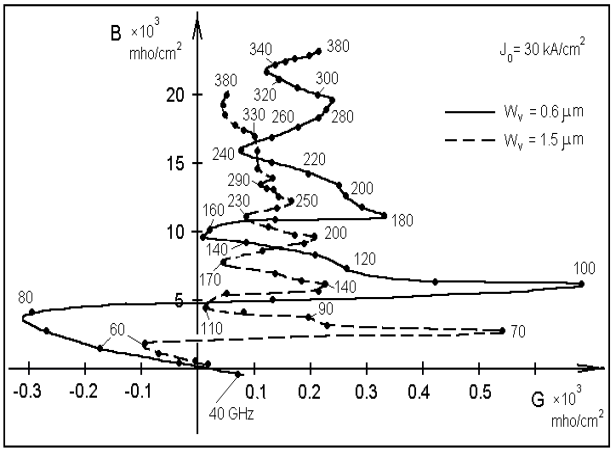

Figure 5. Complex small signal DAR diode admittance (conductance -*G* versus susceptance *B*) for different frequencies and two values of drift layer widths W_v.

features of the DAR diodes. One of the important conclusions of these works concerns of the drift zone width *v* influence to the diode frequency characteristics. It is noted that the diode active properties are produced practically for any drift zone width and this width has an influence on the number of the frequency bands. The larger drift zone provokes more number of frequency bands. Some of these results were obtained by means of the small signal model [5-7]. Other results [8-9] were obtained on the basis of simplified nonlinear model. We suppose that it is necessary to analyze this diode by means of precise model described in section 2.

The DAR diode doping profile was defined the same as in paper [9] for primary analysis to provide the adequate comparison between results which were obtained by two different approaches. Then the accurate analysis for DAR IMPATT diode has been made for different values of *p, n* and *v* region width and the different donor and acceptor concentration level. The analysis showed that the active properties of the diode practically are not displayed for more or less significant width of the region *v*. The same doping profile as in [9] gives the negative conductance for very narrow frequency band only as shown in Fig. 5 in conductance versus susceptance plot.

The solid line of this figure gives dependency for drift layer width W_v = 0.6 μm and the dash line for W_v = 1.5 μm. First dependency displays the diode active properties for one narrow frequency band from 50 GHz up to 85 GHz. Second admittance dependency for W_v = 1.5 μm gives very narrow one frequency band from 40 GHz up to 62 GHz with a very small value of negative conductance *G*. In general the admittance behavior has a damp oscillation character but only first peak lies in negative semi plane. The negative conductance disappears completely for W_v >1.5 μm. All these results have been obtained in assumption of a sufficiently small value of a series resistance R_s = 0.5_{10}-6 Ohm $\cdot$ cm^2. This value was used for all further analysis too.

The main reason of obtained characteristics behavior is the same as for the slow mechanism convergence of the numerical model. The electron and hole avalanches have different transit velocities but they move along the same drift region *v*. It provokes different time delay for the carriers during the transit region movement. The larger width of the region *v* makes delay time more different and the active properties are reduced. That is why we need to reduce the width W_v to obtain necessary negative admittance. This conclusion is contrary to results of the papers [8-9]. The main results obtained by these authors showed the DAR diode active features presence in some frequency bands for different values of *v* region widths from 0.5 μm to 2.0 μm. Our results display the active features of the DAR diode the same profile for some frequency bands in case when the *v*-region width less than 0.5 μm only. The obtained difference could be explained probably by means of approximate numerical model used in paper [9]. One modified Runge-Kutta method was used to mathematical model solve as shown in this paper. However it is known that any explicit numerical method like Runge-Kutta does not have the necessary stability to solve the sufficiently difficult problem for continuity equations (1) with a very sharp dependency of ionization coefficients.

The main reason of this effect is a non-synchronize mechanism of carriersô movement along the drift region. This conclusion is contrary to results of the paper [9]. Our results obtained in this paper display the active features of the DAR diode the same profile for some frequency bands when the width of the *v*-region of the diode less than 0.5 μm only.

One positive idea to increase negative admittance of the diode consists in utilization of the non-symmetric doping profile too. This profile gives some compensation to the asynchronies mechanism which appears into the structure. Taking into account these considerations non-symmetric doping profile diode was analyzed in a wide frequency band. One of the perspective diode structures that was analyzed detail is defined by means of following parameters: the doping level of the *n*-zone is equal to $0.5_{10}17$ cm^{-3}, the doping level of the *p*-zone is equal to $0.2_{10}17$ cm^{-3}, the widths of the two corresponding areas are equal to 0.1 μm and 0.2 μm, accordingly, the width of the drift *v*-region is equal to 0.32 μm, the width of each *p-n* junction was given as 0.02 μm from the technological aspects. This structure provides concentration of electrical field within the two *p-n* junctions and asynchronies mechanism is not displayed drastically yet.

In Fig. 6 the small signal complex admittance i.e. the conductance versus susceptance is presented for the wide frequencies band for DAR diode and for the current density J_0 = 30 kA/cm^2. The DC voltage U_0 is equal to 26.59 V with a small variation from one frequency to other to obtain this value of current density. The first harmonic voltage amplitude is equal to 0.1 V.

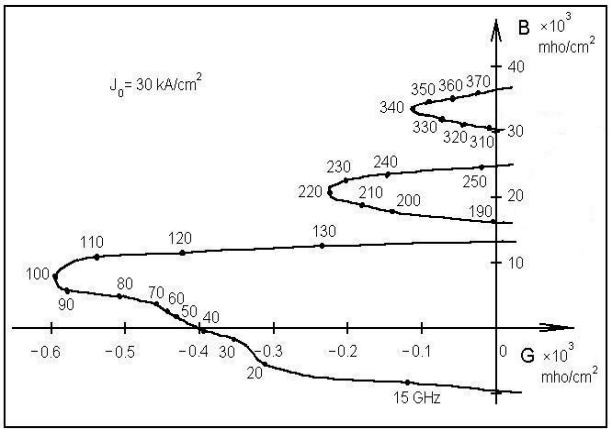

Figure 6. Complex small signal DAR diode admittance for different frequencies and $W_v = 0.32\ \mu$ m.

There are some differences of the DAR diode frequency characteristics from the classical DDR IMPATT diodes (Fig. 4). First of all the DAR diode type has three active bands in the millimeter range (Fig.6) and the DDR diode has only one band. The first active band of the DAR diode is very wide and covers frequency region from 12 to 138 GHz. The second and the third bands near 220 GHz and 340 GHz give the perspective to use this structure for the high frequency generation in the millimeter range too.

We can decide that two superior bands appear from the positive conductance G semi plane (look Fig. 5) as a result of the special conditions making for these bands. This effect gives possibility to use superior frequency bands, first of all the second and the third bands, for the microwave power generation of the sufficient level.

The dependences of conductance $-G$ as the function of the first harmonic amplitude U_1 are shown in Fig. 7 for three frequency bands and for the same value of the current density J_0 = 30 kA/cm^2.

We can decide that two superior frequency bands appear as a result of some special conditions making for these bands. This effect gives us the possibility to use the second and the third frequency bands for the microwave power generation of the sufficient level.

It is obviously that the first frequency band characteristic (f = 90 GHz) has a better behavior. The maximum value of the conductance $-G$ is large and achieves nearly the 600 mho/cm^2 under the small signal. The amplitude dependency for the first band is very soft and this provides a significant value of the generated power.

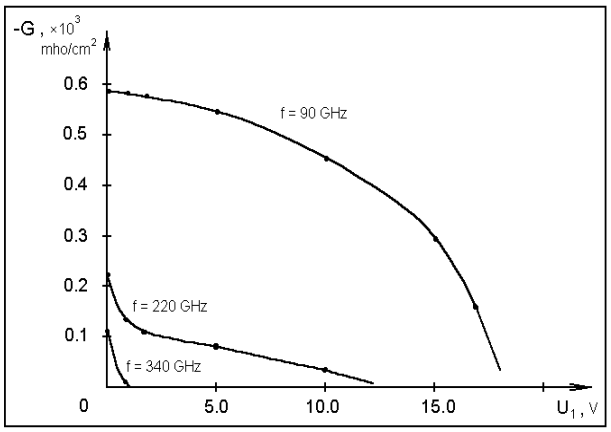

Figure 7. Conductance G dependence as functions of first harmonic amplitude U_1 for different frequency bands.

Nevertheless the second and the third bands (for 220 GHz and for 340 GHz) have the perspective too. The output power dependences for two frequency bands are presented in Fig. 8 as functions of the first harmonic amplitude.

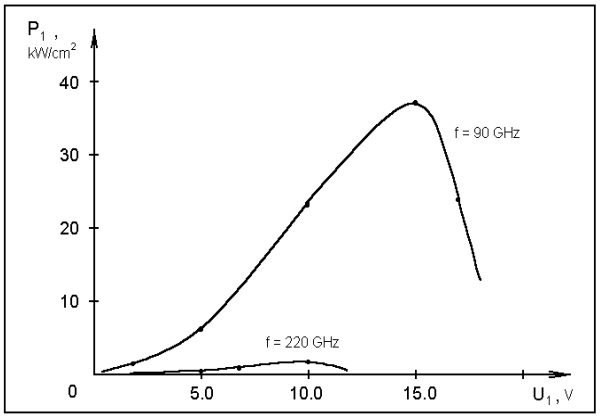

Figure 8. Output power P dependence as functions of first harmonic amplitude U_1 for different frequency bands.

The maximum power density is equal to 37 kW/cm^2 for the first frequency band (90 GHz), and 1.4 kW/cm^2 for the second one (220 GHz). One principal limit of output power for second and third bands is based on the sharp amplitude dependency as shown in Fig. 7. However the possible optimization of the diode internal structure for selected frequency band can improve these characteristics and permits raise the power and the efficiency.

The DAR diode internal structure optimization has been provided below for the second frequency band near 220 GHz and for the third frequency band near 330 GHz separately.

5.2 DAR diode optimization for 220 GHz

The DAR diode internal structure optimization has been provided for the second frequency band near 220 GHz for the feeding current density 30 kA/cm^2. The cost function of the optimization process was selected as output power level for the frequency 220 GHz. The set of the variables for the optimization procedure was composed from five technological parameters of the diode structure: two doping levels for *p* and *n* regions and three widths of *p*, *n* and *v* regions. The optimal values of these parameters were found: doping levels of *n* and *p* zone are equal to 0.42 $_{10}$17 cm^{-3} and 0.28$_{10}$17 cm^{-3} accordingly, the widths of the two corresponding areas are equal to 0.1 μm and 0.2 μm, and the width of the drift *v*-region is equal to 0.34 μm. The results of the complete analysis of small signal admittance for very wide frequency band and for three current density values like 30, 50 and 70 kA/cm^2 are shown in Fig. 9.

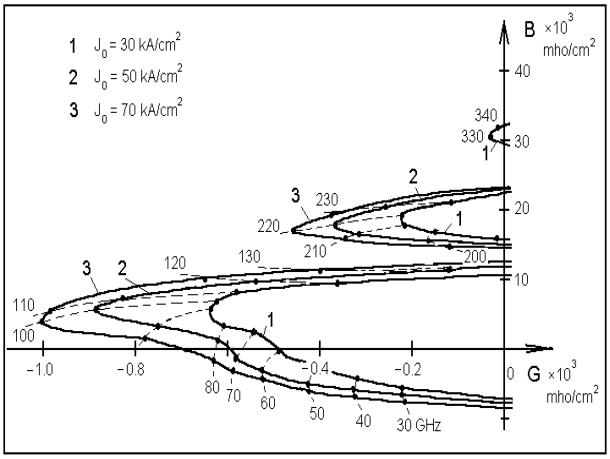

Figure 9. Complex small signal DAR diode admittance optimized for second frequency band for different value of feeding current.

It is clear that the active diode properties for two first bands can be improved when the feeding current density increases. More positive effect was obtained for the frequency 220 GHz because we provided the structure optimization for this frequency exactly.

The characteristics obtained for 220 GHz under a large signal serve as the main result. The amplitude characteristics for the conductance and the output power generated by the diode for this frequency are shown in Fig. 10 and Fig. 11 accordingly. These results have been obtained for three values of the feeding current density.

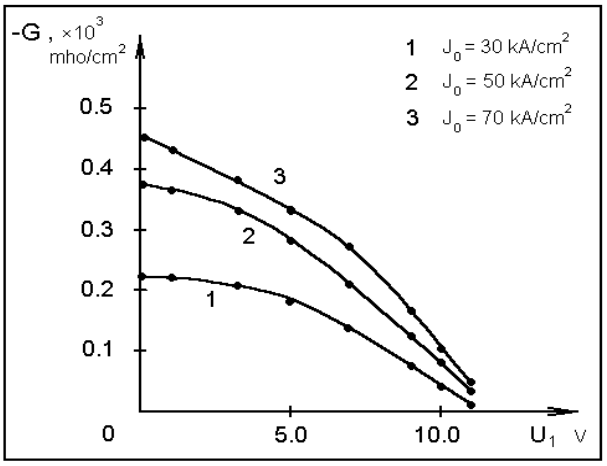

Figure 10. Conductance *G* dependency as function of first harmonic amplitude U_1 for 220 GHz.

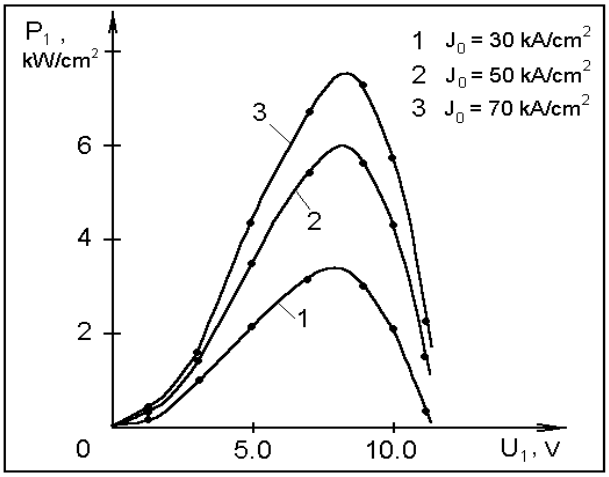

Figure 11. Output generated power *P* dependency as function of the first harmonic amplitude U_1 for 220 GHz.

We can state that a sufficient improvement of power characteristics is observed for this diode structure in comparison with non optimized structure. The maximum values of generated power are equal to 3.3 kW/cm^2 for J_0 =30 kA/cm^2, 6.0 kW/cm^2 for J_0 =50 kA/cm^2 and 7.5kW/cm^2 for J_0 =70 kA/cm^2 accordingly.

5.3 DAR diode optimization for 330 GHz

The results of the diode structure optimization are presented below for frequency 330 GHz and feeding current density 50 kA/cm^2 and 70 kA/cm^2. The small signal admittance optimization for third frequency band is shown in Fig. 12 for two values of current density: 50 and 70 kA/cm^2.

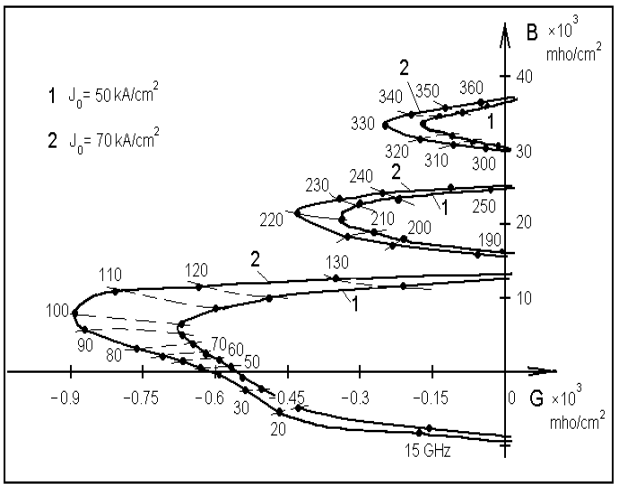

Figure 12. Complex small signal DAR diode admittance optimized for third frequency band for two values of feeding current.

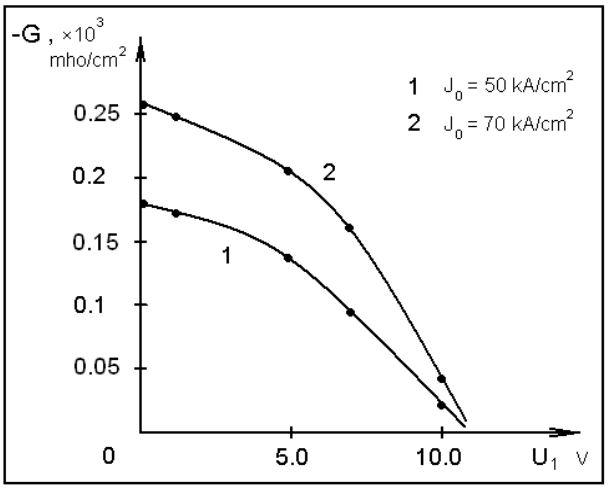

Figure 13. Conductance G dependency as functions of first harmonic amplitude U_1 for f = 330 GHz and for two values of feeding current density.

The cost function of the optimization process was selected as real part of the complex admittance. The set of the optimized variables for the optimization procedure was composed from five technological parameters of the diode internal structure: two doping levels for *p* and *n* regions and three widths of *p*, *n* and *v* regions. The optimal values of these parameters are next: doping levels of *n* and *p* zone are equal to 0.48 $_{10}$17 cm^{-3} and 0.36$_{10}$17 cm^{-3} accordingly, the widths of the two corresponding areas are equal to 0.09 μm and 0.18 μm, and the width of the drift *v*-region is equal to 0.32 μm.

The active diode properties for all frequency bands are improved when the current density increases. More positive effect was obtained for the frequency 330 GHz because the optimization for this frequency. The amplitude characteristics of the conductance for this frequency are shown in Fig. 13 for two values of the current density 50 kA/cm^2 and 70 kA/cm^2.

The conductance characteristic is softer for the current density 50 kA/cm^2 because the diode structure optimization was provided for this current exactly. The characteristics for other feeding current density 70 kA/cm^2 are sharper but correspond to the larger conductance ***ï*** *G*.

The output power dependencies as a function of the first harmonic amplitude U_1 for the frequency f = 330 GHz and for two values of the feeding current density are shown in Fig. 14. These amplitude characteristics show the possibility to obtain a sufficient level of output power of the diode near the 4 kW/cm^2.

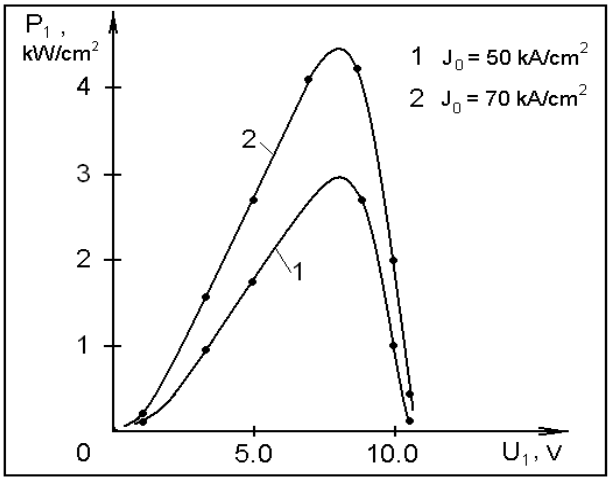

Figure 14. Output generated power P dependency as functions of first harmonic amplitude U_1 for f = 330 GHz and for two values of feeding current density.

6 Conclusion

The numerical scheme that has been developed for the analysis of the different types of IMPATT diodes is suitable for the DAR complex doping profile investigation too. The additional problem that appears for the DAR diode structure analysis is the slower convergence of the numerical model in comparison with the DDR diode analysis.

Some new features of the DAR diode were obtained by the analysis on the basis of nonlinear model on comparing with DDR diode. The principal obtained results contradict to the data that were obtained before on the basis of the approximate

models of the DAR diode. These results show that the diode does not have the active properties in some frequency bands for the sufficiently large drift region. To obtain the negative conductance for some frequency bands we need to reduce the drift layer widths to obtain W_v lesser than $0.5\,\mu$m. Nevertheless the diode has a wide first frequency band generation and two superior frequency bands with sufficient output power level. The optimization of the diode structure gives us the possibility to increase the output power level for high frequency bands. This level can be exceeding in future by means of the special diode structure optimization taking into account necessary feeding current density.

Acknowledgement

This work was supported by the Consejo Nacional de Ciencia y Tecnologia, Mexico under research project CONACYT 164624.

References:

[1] G.I. Haddad, P.T. Greiling, and W.E. Schroeder, Basic principles and properties of avalanche transit-time devices, *IEEE Trans. Microwave Theory Tech.*, MTT-18, 1970, pp. 752-772.

[2] Chang K. (Ed.), *Handbook of microwave and optical components*, John Wile & Sons, N.Y., 1990.

[3] M. Tschernitz, and J. Freyer, 140 GHz GaAs Double-Read IMPATT Diodes, *Electron. Lett.*,Vol. 31, No.7, 1995, pp. 582-583.

[4] W.T. Read, A proposed high-frequency negative resistance diode, *Bell Syst Tech. J*, Vol. 37, 1958, pp. 401-446.

[5] B. Som, B.B.Pal, and S.K.Roy, A small signal analysis of an IMPATT device having two avalanche layers interspaced by a drift layer, *Solid-State Electron.*, Vol. 17, 1974, pp. 1029-1038.

[6] D.N. Datta, B.B.Pal, Generalized small signal analysis of a DAR IMPATT diodeò, *Solid-State Electron*, Vol. 25, No. 6, 1982, pp. 435-439.

[7] D. N. Datta, S. P. Pati, J. P. Banerjee, B. B. Pal, and S. K. Roy, Computer analysis of DC field and current-density profiles of DAR IMPATT diode. IEEE Trans Electron Devices, Vol. ED-29, No. 11, 1982, pp. 1813-1816.

[8] S.P. Pati, J.P. Banerjee, and S.K. Roy, High frequency numerical analysis of double avalanche region IMPATT diode, *Semicond Sci Technol*, No. 6, 1991, pp. 777-783.

[9] A.K. Panda, G.N. Dash, and S.P. Pati, Computer-aided studies on the wide-band microwave characteristics of a silicon double avalanche region diode, *Semicond Sci Technol*, No. 10, 1995, pp. 854-864.

[10] A. M. Zemliak, S. Cabrera, Numerical Analysis of a DAR IMPATT diode, *J Comput Electron*, Vol. 5, No. 4, December 2006, pp. 401-404.

[11] W.N. Grant, Electron and hole ionization rates in epitaxial silicon at high electric fields, *Solid-State Electron*., Vol. 16, No. 10, 1973, pp. 1189-1203.

[12] C. Jacoboni, C. Canali, G. Ottaviani, A review of some charge transport properties of silicon, *Solid-State Electron*, Vol. 20, 1977, pp. 77-89.

[13] C. Canali, C. Jacoboni, G. Ottaviani, High field diffusion of electrons in silicon, *Appl Phys Lett*, Vol. 27, 1975, p. 278.

[14] F. Nava, C. Canali, L. Reggiani, D. Gasquet, J.C. Vaissiere, and J.P. Nougier, On diffusivity of holes in silicon, *J Appl Phys*, Vol. 50, 1979, p. 922.

[15] A.M. Zemliak, Difference scheme stability analysis for IMPATT-diode design, *Izv. VUZ Radioelectronika*, Vol. 24, No. 8, 1981, pp. 831-834.

[16] A. Zemliak, S. Khotiaintsev, and C. Celaya, Complex nonlinear model for the pulsed-mode IMPATT diode, *Instrumentation and Development*, Vol. 3, No. 8, 1997, pp. 45-52.

[17] A. Zemliak, C. Celaya, R. Garcia, Active layer parameter optimization for high-power Si 2 mm pulsed IMPATT diode, *Microwave Opt. Technol. Lett.*, Vol. 19, No. 1, 1998, pp. 4-9.